Spectromicroscopy Study of Intercalation and Exfoliation in Polypropylene/Montmorillonite Nanocomposites

ARTICLE *in* THE JOURNAL OF PHYSICAL CHEMISTRY B · SEPTEMBER 2009

Impact Factor: 3.3 · DOI: 10.1021/jp9049999 · Source: PubMed

6 AUTHORS, INCLUDING:

Zulima Martin
Spanish National Research Council
13 PUBLICATIONS **216** CITATIONS
SEE PROFILE

I. Jiménez
Spanish National Research Council
114 PUBLICATIONS **2,000** CITATIONS
SEE PROFILE

Harald Werner Ade
North Carolina State University
353 PUBLICATIONS **8,639** CITATIONS
SEE PROFILE

Daniel Hernandez cruz
Universidad Autónoma de Chiapas (UNACH)
36 PUBLICATIONS **343** CITATIONS
SEE PROFILE

Spectromicroscopy Study of Intercalation and Exfoliation in Polypropylene/Montmorillonite Nanocomposites

Zulima Martín,*,† Ignacio Jiménez,‡ M. Ángeles Gómez,† Harald W. Ade,§ David A. Kilcoyne,|| and Daniel Hernádez-Cruz⊥,#

Instituto de Ciencia y Tecnología de Polímeros, ICTP-CSIC, Juan de la Cierva 3, 28006 Madrid, Spain, Instituto de Ciencia de Materiales de Madrid, ICMM-CSIC, Campus de Cantoblanco, 28049 Madrid, Spain, Department of Physics, North Carolina State University, Raleigh, North Carolina 27695, Advanced Light Source, Lawrence Berkeley National Laboratory, Berkeley, California 94720, and BIMR—Chemistry Department, McMaster University, Hamilton, Ontario, L85 4M1, Canada

Received: May 28, 2009; Revised Manuscript Received: July 7, 2009

We present a combined study by X-ray diffraction, scanning electron microscopy (SEM), transmission electron microscopy (TEM), and scanning transmission X-ray microscopy (STXM) of the successful formation of nanocomposites of polypropylene with montmorillonite by melt processing, providing a complete picture of the intercalation and exfoliation processes taking place. The nanocomposites contained 5 wt % of an organically modified montmorillonite, and different amounts of polypropylene-*graft*-maleic anhydride, used as a polar compatibilizer. Microscopy reveals a complex morphology, with partial intercalation/exfoliation, which depends on the concentration of compatibilizer. STXM spectromicroscopy provides direct information of the presence of different polymer components at the polymer—silicate interfaces and details on the intercalation mechanism.

Introduction

The production of clay—polymer nanocomposites is an active area of research which benefits from the high surface area ratio of nanoclay particles to greatly improve the thermomechanical properties of the polymer matrix, even with low filler contents. The success in the development of clay—polymer nanocomposites requires two key conditions: first, achieving a correct dispersion of nanoparticles in the matrix in order to obtain a high fraction of interfacial clay—polymer region within the material, and second, controlling the interfacial interactions between silicate particles and the polymer matrix, so that highly interacting polymer chains can either intercalate between the silicate layers or even break the stacking of the basal planes to induce exfoliation.[1−4] A detailed study of these two conditions requires the use of microscopic and spectromicroscopic techniques. The characterization of the nanoparticle dispersion and the composite nanostructure can be obtained directly from analysis of the micrographs. However, the study of the interfacial clay—polymer interactions requires the use of spectromicroscopies combining chemical sensitivity with nanometric resolution to distinguish the components present at the interfaces and how they affect the intercalation or exfoliation of clay layers. In our study, we have combined state-of-the-art spectromicroscopy achieved using scanning transmission X-ray microscopy (STXM) with higher spatial resolution transmission electron microscopy (TEM) and scanning electron microscopy (SEM) to address this problem and provide direct observations of the effect of compatibilizing agents in the intercalation and exfoliation of nanoclays.

In this work, we have preparated isotactic polypropylene/montmorillonite composites from the melt, since this processing method is the most attractive for industrial applications.[5−9] Montmorillonite (MMT) is the most common layered silicate for the preparation of nanocomposites because of its high aspect ratio, large surface area, and surface reactivity. Its structure consists of the stacking of aluminosilicate layers ∼1 nm thick, with a regular spacing between them of ∼1.5 nm. Their high cation exchange capacity offers a way of modifying the interlayer spacing to make it larger and more compatible with polymers. However, unlike polymers with polar groups like polyamides,[2,5,10−12] in nonpolar polymers like polypropylene (PP) the organic modification of the clay does not produce large enough clay—polymer interfacial interactions to achieve a good clay dispersion and hardly leads to mixed structures.[13−18] To improve the polymer—filler interactions, polypropylene-*graft*-maleic anhydride (PP-*g*-MA) has been added because it is a general-use common compatibilizer for this purpose.[19−22] It has been selected on the basis of its chemical nature, molecular weight and grafting content.

Experimental Section

Materials. The polypropylene (PP) used as matrix was an isotactic homopolymer, with a polydispersity of 4.77, provided by REPSOL-YPF. It is characterized by an isotacticity of 95%, determined by solution NMR, and a viscosity average molecular weight of 179,000 g/mol, obtained by intrinsic viscosity measurements by using a modified Ubbelholde viscometer in decalin solutions at 135 °C. A concentration of 0.1 g/dL was used, and the measurements were carried out under nitrogen atmosphere. The intrinsic viscosity—molecular weight relationship is given by $[\eta] = 1.10 \times 10^{-4} \times M_v^{0.80}$.[23] The clay nanoparticles were organically modified montmorillonite (MMT) Cloisite 20A (C20A) obtained from Southern Clay Products.

* Corresponding author. E-mail: zmartin@ictp.csic.es.
† ICTP-CSIC.
‡ ICMM-CSIC.
§ North Carolina State University.
|| Lawrence Berkeley National Laboratory.
⊥ McMaster University.
This author is currently at Universidad Autonoma de Chiapas, Chiapas, Mexico.

10.1021/jp9049999 CCC: $40.75
Published on Web 07/22/2009

The average dry particle size is 8 μm and is composed of millions of individual platelets that only appear separated after a good dispersion in a polymer or a liquid dispersant. The individual platelets are typically 1 nm in thickness, with an aspect ratio larger than 50. It is modified with *N*,*N*-dimethyl dihydrogenated tallow quaternary ammonium chloride. Tallow is a mixture of octadecyl (major component (>60%)), hexadecyl and tetradecyl. The modifier concentration is 95 mequiv/100 g clay, with a weight lost on ignition of 38%, and the interlayer spacing, determined by XRD, is $d_{001} = 2.52$ nm. As compatibilizer, we used a polypropylene-*graft*-maleic anhydride (PP-*g*-MA) with a maleic anhydride content of 0.42 wt % and a viscosity average molecular weight of 83,500 g/mol, EXXELOR PO1015 provided by EXXON.

Preparation of PP-MMT Composites. Composites were prepared by melt blending the components in a Haake Rheomix 600 internal mixer attached to a Haake Rheocord 90 corotating twin screw mixing chamber. A temperature of 190 °C, mixing time of 5 min, and rotor speed of 100 rpm were determined to be the more convenient processing conditions. The clay loading in all the composites was 5 wt %, which is within the optimal range of filler contents for mechanical performance.[15,17,18,24,25] Three composites were prepared: (i) without any compatibilizer, i.e. containing 95 wt % PP and 5 wt % C20A, which is labeled as PP/C20A (95/5), (ii) with a 1:1 weight ratio of clay:compatibilizer, labeled as PP/C20A/PP-*g*-MA (90/5/5), and (iii) with a 1:3 ratio of clay:compatibilizer, labeled as PP/C20A/PP-*g*-MA (80/5/15).[9,18,19] Films of the nanocomposite material were compression molded at 100 Mbar by heating the pellets at 190 °C for 5 min with subsequent quenching of the formed film between water-cooled metal plates.

Characterization of PP-MMT Nanocomposite Structure. ***XRD.*** X-ray diffraction (XRD) was used to characterize the changes in the clay interlayer spacing induced by the polymer intercalation. XRD patterns were obtained at room temperature using a Philips PW 1050/70 diffractometer, at 1°/min in a 2θ range between 2 and 35° using Ni-filtered Cu Kα radiation.

SEM and TEM. The composite morphology and the nanoclay dispersion were examined by SEM and TEM. SEM images were obtained with a Philips XL30 ESEM, using an accelerating voltage of 25 kV. The polymer samples were cryofractured from film specimens and coated with a ~5 nm Au/Pd overlayer to avoid charging during electron irradiation. TEM images were obtained with a Philips Tecnai 20 microscope. Ultrathin sections, 50−100 nm in thickness, were cryogenically microtomed with a diamond knife at ~−60 °C. Sections were collected on copper TEM grids.

STXM. Scanning transmission X-ray microscopy (STXM) measurements were conducted using the STXM at BL5.3.2 of the Advanced Light Source at Lawrence Berkeley National Laboratory.[26] This combines microscopic and spectroscopic information at the nanoscale, to enable the identification and chemical composition at the nanocomposite interfaces.

BL 5.3.2 STXM provides images with ~40 nm spatial resolution for X-ray photons of 250−600 eV, with an energy resolution of about 0.1 eV. The energy range includes the most important absorption edges in polymer chemistry, C(1s) at 280 eV, N(1s) at 400 eV and O(1s) at 520 eV. The basis for contrast in the images is the elemental differential X-ray absorption through components of the composite material. A Fresnel zone plate is used to focus the monochromatic X-rays to a nanometric spot, and the whole sample is mapped with nanometric resolution by X-ray absorption near edge spectroscopy (XANES or NEXAFS). Images are acquired by raster scanning the sample at the focal spot while detecting the flux of transmitted X-rays. TEM grid-supported samples were mounted in the sample chamber which was evacuated to 0.3 mbar and subsequently refilled with 1/3 atm of helium. The transmitted X-ray intensity through the film was recorded using a scintillator and photomultiplier tube and measured as a function of photon energy and position. Spectra are obtained by successively stepping the X-ray energy through a spectral region while recording point, line, or image data. Image sequences, used to provide detailed chemical mapping, were converted to chemical component maps using pixel-by-pixel curve fitting with suitable XANES spectra from reference components. Details about this instrument and experiment can be found elsewhere.[26]

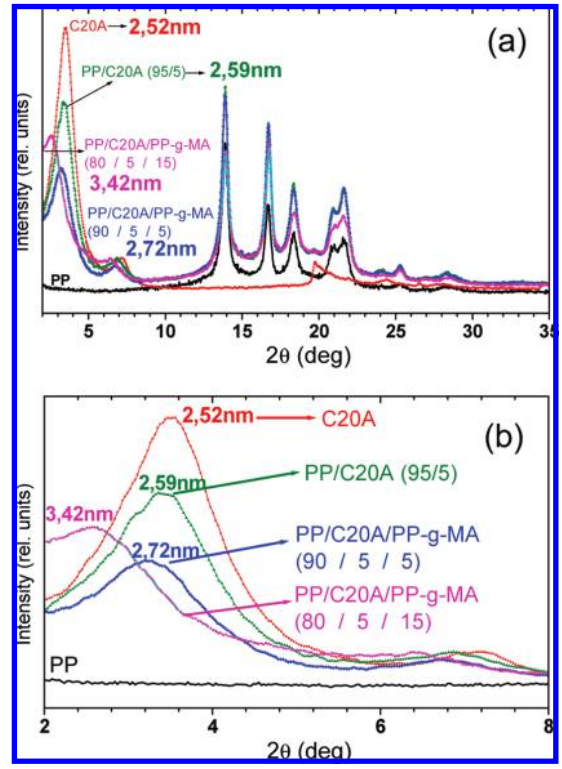

Figure 1. XRD patterns for pristine PP and clay and for Nanocomposites. Inset number denotes the d_{001} of clay.

Results and Discussion

(a) Evaluation of the Intercalation Capability of Polymers Chains in PP/MMT and PP/MMT/PP-*g*-MA Composites by X-ray Diffraction. As mentioned earlier, one of the keys to obtain a polymer−clay nanocomposite is to achieve a satisfactory dispersion of the nanoclay in the polymer matrix. This requires an efficient interaction between nanoclay and matrix allowing the polymer chains to insert within the interlayer of the montmorillonite structure leading to intercalated or exfoliated structures. Figure 1 shows XRD patterns of both pristine PP and C20A, and of the prepared composites. It is clearly seen in Figure 1(a) that neither the presence of C20A and PP-*g*-MA nor the composite preparation method alters the monoclinic α structure of isotactic polypropylene (i-PP) since the composites maintain the same diffraction peaks as the reference i-PP.[27,28] The level of intercalation in C20A was evaluated from the variations of the clay interlayer spacing, which is derived from the 2θ position of the (001) diffraction peak shown in Figure 1(b). Pristine clay has a *d* spacing (d_{001}) of 2.52 nm. Even if the presence of the diffraction peak in the composites indicates that the clay was not fully exfoliated, the increase in the

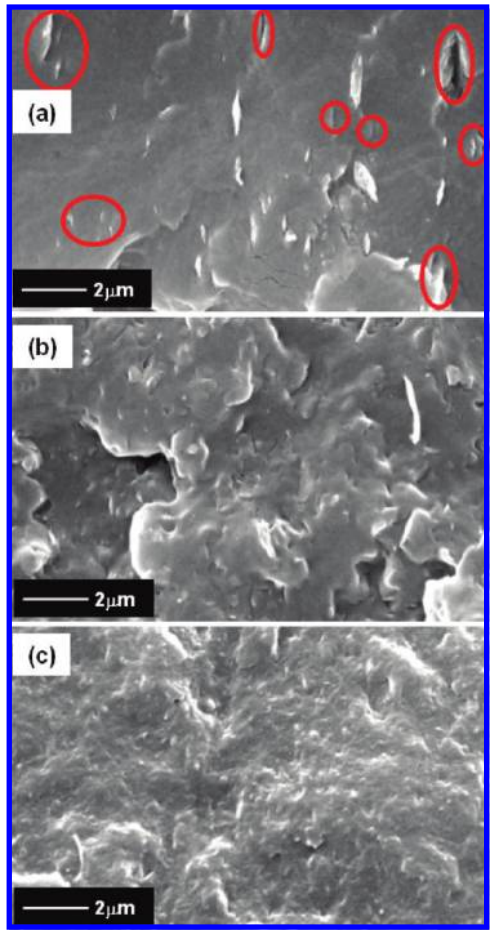

Figure 2. SEM images at 25 kV acceleration voltage of the fracture surface of (a) PP/C20A (95/5), (b) PP/C20A/PP-*g*-MA (90/5/5), and (c) PP/C20A/PP-*g*-MA (80/5/15).

d-spacing observed for all composites indicates the formation of intercalated structures.[3] Without compatibilizer the interlayer spacing of the C20A increases slightly from 2.52 ± 0.05 nm to 2.59 ± 0.05 nm. With the use of PP-*g*-MA as compatibilizer, the interlayer distance increases to 2.72 ± 0.05 nm and 3.42 ± 0.05 nm for 5 and 15 wt % of compatibilizer, respectively. This implies that the intercalation capability of the polymers increases with increasing their polarity, in agreement with other work.[12,16,17] From the shift of the diffraction peaks, we conclude that the nanocomposites have an intercalated structure. From the decrease in the intensity of the basal diffraction peak in the nanocomposites it is clear that the intercalation is not taking place by a parallel displacement of the silicate layers that maintains an ordered structure, but rather by a disordered intercalation and/or by a mixture of intercalation and exfoliation mechanisms.[17,29] Since XRD does not allow a more detailed characterization of the structure of the nanocomposites, we searched for additional information by microscopy and spectromicroscopy studies.

(b) Characterization of the Clay Dispersion and Morphology by Electron Microscopies. To discern at a microscopic level the mechanisms of intercalation and exfoliation induced by the interaction of the polymer chains with the nanoclay, a detailed characterization of the clay dispersion and nanocomposite morphology was obtained by SEM and TEM.

Figure 2 shows SEM images of the fracture surfaces of the nanocomposites where the brightest areas correspond to C20A montmorillonites, as verified by EDX microanalysis (not shown here). Without compatibilizer, Figure 2(a), there is minimal dispersion of the C20A as evident in the imaged structure. The nanoclay appears in stacks of different sizes. The presence of cracks (marked in the figure) corresponds to the location of MMT particles that have detached from the PP matrix during the fracture, and indicates that the adhesive energy between PP and C20A is much lower than the clay fracture energy. With the addition of PP-*g*-MA there is not only an improvement in the dispersion of the clay but also an increase in the adhesion between clay and matrix evidenced by the absence of cracks. With 5 wt % of compatibilizer, Figure 2(b), we still observe some stacks of MMT which are absent after incorporation of 15 wt % of compatibilizer, as shown in Figure 2(c). In this latter case C20A-MMT is hardly observed, suggesting exfoliation of the clay.

Additional information on the structure of the nanocomposites was obtained with the use of TEM, as shown in Figure 3. At the micrometer scale (top row, scale bar 1 μm) the information obtained is similar to the SEM images of Figure 2 but better defined, not only because of the higher resolution of TEM but also because the transmission images are not affected by the morphology of the fracture surface. The distribution of nanoclay particles and stacks previously observed by SEM is confirmed.

From the medium resolution images, shown in the central row of Figure 3 with a scale bar of 200 nm, we have made a statistical analysis of the size and morphology of the MMT stacks, which is summarized in Table 1. In the absence of compatibilizer (left panel) there is not a good distribution of the nanoclay. C20A appears in stacks with an average length of 700 ± 200 nm and an aspect ratio ranging between 20 and 140. Nevertheless there are intercalated regions and the stacks are smaller than in pristine montmorillonite, with typical dry particle size 2−13 μm.[30] By adding the PP-*g*-MA compatibilizer, the nanoclay dispersion improves. With 5 wt % of compatibilizer, exfoliated single layers are clearly visible, together with intercalated regions in parallel planes (middle panel, central row), hence evidencing the presence of a mixed morphology containing a few small stacks and exfoliated layers. Although some stacks are still observed, these are much smaller in number and size (see Table 1) than without compatibilizer. With the increase of PP-*g*-MA content to 15 wt % the nanoclay dispersion further improves. The presence of single-layer nanoclay platelets dominates the TEM images, and only a few stacks can be observed, as appears in Figure 3 (right panel, central row). The small number of stacks explains the decreased intensity of the diffraction peak at 3.42 nm shown in Figure 1 for this sample.

The bottom row of Figure 3 shows TEM images at the highest magnification (scale bar of 50 nm). Without compatibilizer (left) part of one stack is apparent in the image. The clay platelets tend to separate from the stack in parallel, and intercalated regions are observed. With 5 wt % of compatibilizer intercalated regions and isolated layers are just visible. With 15 wt % of compatibilizer we can clearly see how the nanoclay layers have separated completely from the stack. TEM images indicate that in the system PP/C20A/PP-*g*-MA exfoliation takes place by a delamination of the montmorillonite starting from the edge of the layer and fanning out, as other authors have proposed before,[31] and not by removal of montmorillonite platelets, sheet by sheet, as an independent process of intercalation, as other authors suggested.[6,29] Mechanistically, the polymer chains insert among superficial sheets covering 5−10 layers, forcing this smaller platelet sized stack to detach from the edge of the layer. When the stacks are reduced, the polymer chains repeat the same process sheet by sheet from the outer layer. From the TEM images obtained with the highest magnification a new statistical

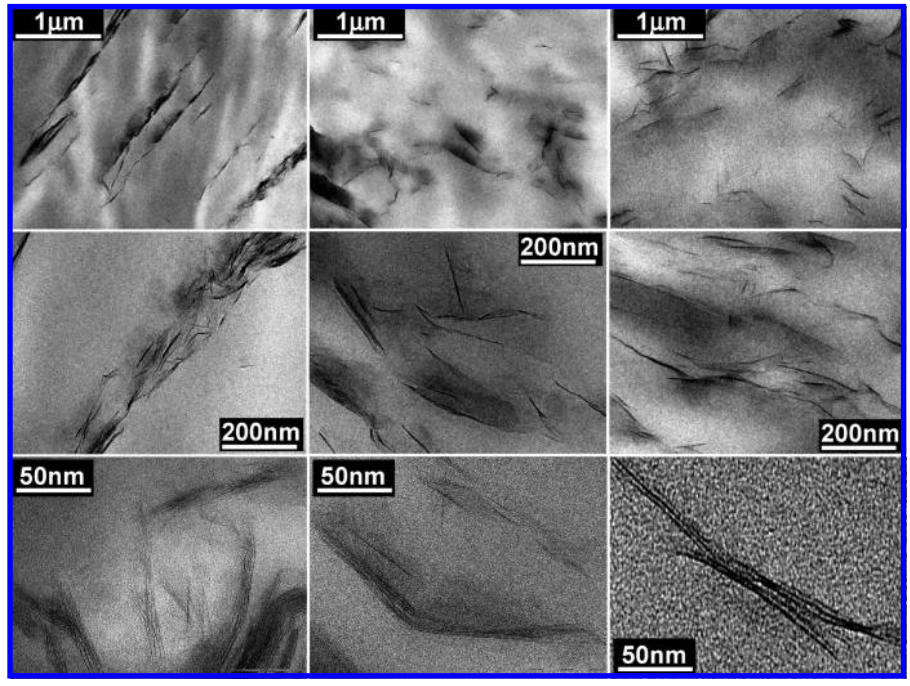

Figure 3. TEM images of the nanocomposites PP/C20A (95/5) (left column), PP/C20A/PP-*g*-MA (95/5/5) (middle column) and PP/C20A/PP-*g*-MA (80/5/15) (right column) at different magnifications (low: first row, medium: second row, high: third row).

TABLE 1: C20A (5 wt %) Average Dimensions from the TEM Images as a Function of Compatibilizer Content

	interlayer distance (nm)	
compatibilizer wt %	from TEM	from XRD
0	2.4 ± 0.3	2.59 ± 0.05
5	3.0 ± 0.4	2.72 ± 0.05
15	3.3 ± 0.8	3.42 ± 0.05

TABLE 2: Interlayer Distances of PP/C20A/PP-*g*-MA

compatibilizer wt %	length (nm)	aspect ratio
0	700 ± 200	80 ± 60
5	130 ± 80	8 ± 6
15	170 ± 90	no stacks found

analysis of the interlayer distance of C20A in the nanocomposites can be evaluated, which is summarized in Table 2. The results are in agreement with the XRD data, but clearly indicate that the interlayer spacing derived from XRD is just an average value for a mixed morphology of intercalated and exfoliated clays, and not an actual value for a well-defined interlayer distance in regularly intercalated montmorillonites. As the TEM images show, the dispersion of clay exhibits different morphologies, including occasional stacks of nonintercalated C20A, intercalated regions with a nonuniform separation of the layers, and exfoliated single layers isolated from any stack. The degree of exfoliation increases with the PP-*g*-MA content, indicating that it is controlled by the amount of polar groups incorporated to the nonpolar polypropylene matrix.

(c) Spectromicroscopy of the Clay−Montmorillonite system by STXM. STXM spectromicroscopy, which combines nanometric spatial resolution with chemical contrast in the images, has been used to observe directly the presence of different polymer components at the polymer−silicate interfaces. Although this is a difficult problem for polymer components which are chemically rather similar, as is the case here, the high chemical sensitivity of STXM has shown its ability to discern similar components in polymer blends.[32−34]

To perform the STXM analysis reference XANES spectra from the pure component materials of the nanocomposites are required. The C(1s) XANES references are displayed in Figure 4(a). Since the intensity corresponding to the clay is much lower than those corresponding to the polyolefins, the spectra are normalized to the maximum height for comparison purposes. The scaling factors to obtain the same height are indicated in the figure. The bottom curve corresponds to the PP matrix, showing the characteristic peak of polyolefins at 288 eV in σ^*_{C-H} region, at the onset of the σ^* states.[35] The C(1s) spectrum from PP-*g*-MA is similar, indicating that the maleic anhydride content of 0.42 wt % is not enough to provide a noticeable signal at the carbon absorption edge. The topmost curve is from the C20A montmorillonite. Although the exchanged organic cation of C20A is supposed to contain only alkyl chains, experimentally we find the presence of a peak at 285 eV, typical of $\pi^*_{C=C}$ states, that evidence the presence of double bonds in the hydrocarbonated chains of the organic modification of the MMT.

To obtain chemical contrast in the STXM images, a complete sequence of images at photon energies encompassing the C(1s) region are recorded corresponding to a typical XANES energy scan. In this way, each pixel, representing a morphological and spatial dimension, contains a full XANES spectrum that can be curve fitted to the previously acquired XANES reference spectra, thus providing the contribution of each component material at micrometer/nano scale. A chemical composition map obtained in this way, using C(1s) edge data from 272 to 320 eV, is shown in Figure 4(b) for the PP/C20A/PP-*g*-MA (80/5/15) sample. The different colors represent the contribution of the component materials: green regions represent PP and blue ones the C20A-MMT. We observe a homogeneous clay dispersion in the PP matrix although some bigger particles indicate the presence of small stacks of C20A. Since the C(1s) XANES spectra from the compatibilizer and the PP matrix are essentially identical, it is not possible to distinguish any difference in their spatial distribution from the C(1s) images.

However, we can obtain contrast between PP and compatibilizer at the O(1s) edge due to the differential contrast of

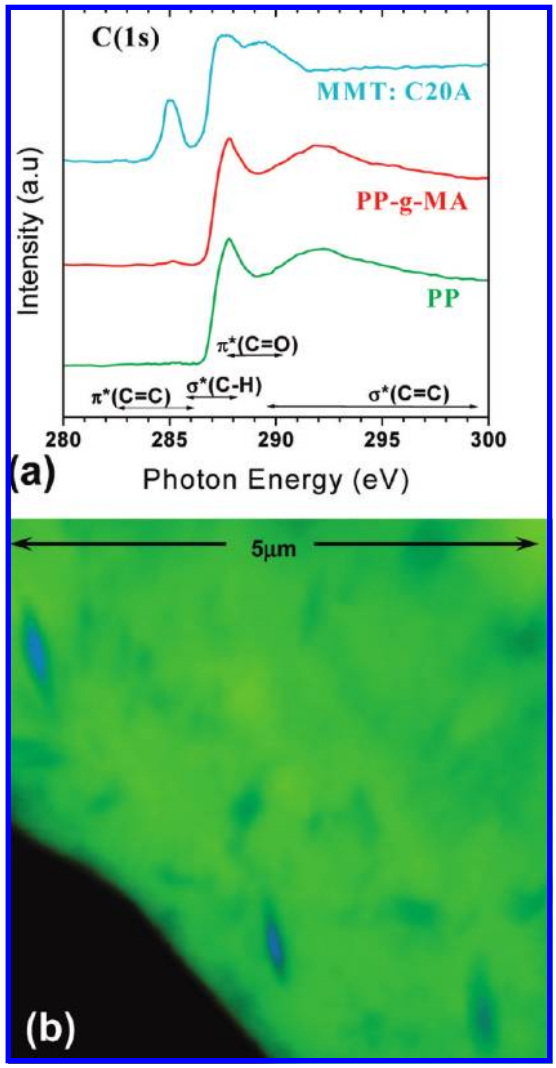

Figure 4. (a) NEXAFS spectra at the C(1s) edge of pristine components: PP, PP-*g*-MA and C20A. (b) 5 μm by 5 μm STXM composition map of PP/C20A/PP-*g*-MA (80/5/15) recorded from 272 eV up to 320 eV.

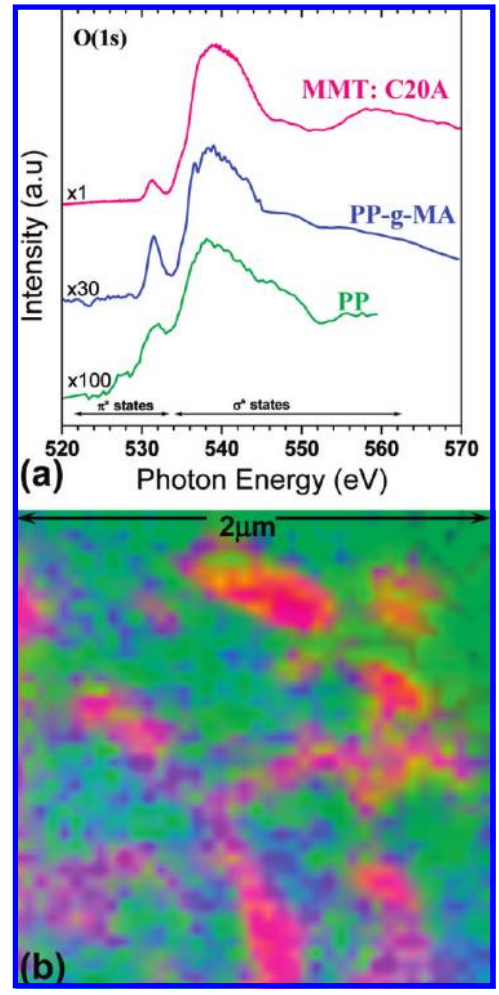

Figure 5. (a) NEXAFS spectra at the O(1s) edge of pristine components: PP, PP-*g*-MA and C20A. (b) 2 μm by 2 μm STXM composition map of PP/C20A/PP-*g*-MA (80/5/15) recorded from 500 eV up to 570 eV.

STXM. Figure 5(a) shows XANES spectra measured at the O(1s) edge from the reference components, normalized to the maximum height for comparison purposes. The O(1s) absorption signal in PP is very low (the spectrum, Figure 5(a), has been scaled by a factor of 100), as PP does not intrinsically contain any oxygen. This yields an ill-defined XANES spectrum, and any spectral signature present is assigned to environmental contamination due to the hygroscopic character of PP. The PP-*g*-MA compatibilizer contains structural oxygen, showing a well-defined peak at 532 eV related to the C═O bonds of the maleic group. The C20A-MMT spectrum is the most intense and is dominated by the Si−O signal in the silicate.

Figure 5(b) shows a high resolution (2 μm × 2 μm) chemical composition map from the PP/C20A/PP-*g*-MA (80/5/15) sample derived by fitting the O(1s) image sequence taken from 500 to 570 eV to the spectra of the pure components. Now, we can perfectly identify the presence of the three components, which is represented with different colors: green regions correspond to PP, blue regions to PP-*g*-MA compatibilizer, and magenta regions to C20A-MMT. Note that a pixel can contain various component materials since the pixel size was 40 nm. From the images it is clear the presence of a few orange or yellow pixels, representing the presence of PP (green) and MMT (magenta) in the same pixel area, a dominant number of purple pixels corresponding to the mixing of MMT (magenta) and PP-*g*-MA (blue) in the same area, and also different green tonalities corresponding to the mixture of PP with the compatibilizer. Due to the small oxygen signal of the PP, the composition map for the PP has a very low S/N ratio. This results in the appearance of the green signal as a background.

Three direct observations of importance can be made from Figure 5. First, the PP matrix and the compatibilizer are mixed homogeneously, without apparent phase separation away from any clay. Second, although both PP and the compatibilizer appear surrounding the nanoclay, there is a clear dominance of PP-*g*-MA in the vicinity of the MMT, hence confirming the polar interaction between PP-*g*-MA and the clay. Third, there are several MMT particles that appear completely in purple color, e.g. in the bottom-left part of the image, which correspond to clay particles fully intercalated by the compatibilizer, but there are no MMT particles fully in yellow or orange color. The yellow-orange pixels appear only in the contact regions between MMT and PP, but never in the center of the clay particle, indicating that the nonpolar PP is not capable of complete intercalation.

Conclusions

The successful formation of a nanocomposite of the C20A montmorillonite in the PP matrix by melt processing has been

examined by different techniques to provide a complete picture of the intercalation and exfoliation processes. XRD patterns showed that intercalation of the polymer chains in the clay takes place when a PP-*g*-MA compatibilizer is used, because the C20A interlayer spacing expands from 2.52 nm up to 3.42 nm in the composites containing 15 wt % of compatibilizer. Without compatibilizer the increase of interlayer spacing is very low.

SEM images from fractured surfaces indicate that both the clay dispersion and the adhesion between polymer matrix and clay are much better with the addition of the addition of a compatibilizer and provide a picture of how the intercalation takes place by opening the edges of the clay particles fanning out, and proceeds toward the particle center to eventually produce the layer exfoliation. The TEM results indicate that the XRD interlayer spacing is only an average value over a complex morphology, with unperturbed clay particles, intercalated particles and exfoliated layers. Increasing amounts of the polar compatibilizer PP-*g*-MA result in a decrease of the particle aspect ratio, and increase of the average interlayer distance, and an increase of the exfoliation degree.

Finally, spectromicroscopy STXM images indicate that the compatibilizer surrounds preferentially the nanoclay due to polar interactions, and that under favorable processing conditions the polymer chains with polar groups intercalate the nanoclay from the edges. This idea has been proposed previously[7,31] and here we show direct experimental evidence that confirms this process.

Acknowledgment. This work has been supported by the I3P-CSIC predoctoral program, and has been partially financed by project FOREMOST (Contract No. NMP3-CT-2005-515840) from the EU FP6 programme, and the Spanish MICINN for national project (MAT2006-13167-C01). We are indebted to J. González-Casablanca and R. Castro from Universidad Rey Juan Carlos (URJC) of Madrid for their assistance in the use of the TEM. We also acknowledge the assistance of Sufal Swaraj and Benjamin Watts at the BL-5.3.2 STXM of the ALS, which is supported by the Director of the Office of Science, Department of Energy, under Contract No. DE-AC02-05CH11231. Work at NCSU is supported by DOE Grant DE-FG02-98ER45737.

References and Notes

(1) Vaia, R. A.; Jandt, K. D.; Kramer, E. J.; Giannelis, E. P. *Macromolecules* **1995**, *28*, 8080–8085.
(2) Ray, S. S.; Okamoto, M. *Prog. Polym. Sci.* **2003**, *28*, 1539–1641.
(3) Thostenson, E. T.; Chou, C. L. T.-W. *Compos. Sci. Technol.* **2005**, *65*, 491–516.
(4) Kalaitzidou, K.; Fukushima, H.; Miyagawa, H. *Polym. Eng. Sci.* **2007**, *47*, 1796–1803.
(5) Vaia, R. A.; Giannelis, E. P. *Macromolecules* **1997**, *30*, 8000–8009.
(6) Xu, W.; Guodong, L.; Wang, W.; Tang, S.; He, P.; Pan, W.-P. *J. Appl. Polym. Sci.* **2005**, *88*, 3225–3231.
(7) Modesti, M.; Lorenzetti, A.; Bon, D.; Besco, S. *Polymer* **2005**, *46*, 10237–10245.
(8) Park, J. U.; Choi, Y. S.; Cho, K. S.; Kim, D. H.; Ahn, K. H.; Lee, S. J. *Polymer* **2006**, *47*, 5145–5153.
(9) Rzaev, Z. M. O.; Yilmazbayhan, A.; Alper, E. *Adv. Polym. Sci.* **2007**, *26*, 41–55.
(10) Okada, A.; Fukushima, Y.; Kawasumi, M.; Inagaki, S.; Usuki, A.; Sugiyama, S.; Kurauchi, T.; Kamigaito, O. U.S. Patent 4,739,007, Toyota Motor Co., Japan, 1988.
(11) Sung, Y. T.; Kim, Y. S.; Lee, K.; Dim, W. N.; Lee, H. S.; Sung, J. Y.; Yoon, H. G. *Polym. Eng. Sci.* **2007**, *47*, 1671–1677.
(12) Mittal, V. *J. Appl. Polym. Sci.* **2008**, *107*, 1350–1361.
(13) Hasegawa, N.; Kawasumi, M.; Kato, M.; Usuki, A.; Okada, A. *J. Appl. Polym. Sci.* **1998**, *67*, 87–92.
(14) Rapoport, L.; Nepomnyashchy, O.; Verdyan, A.; Popovitz-Biro, R.; Volovik, Y.; Ittah, B.; Tenne, R. *Adv. Eng. Mater.* **2004**, *6*, 44–48.
(15) Jang, B. N.; Wang, D.; Wilkie, C. A. *Macromolecules* **2005**, *38*, 6533–6543.
(16) Kim, D. H.; Fasulo, P. D.; Rodgers, W. R.; Paul, D. R. *Polymer* **2007**, *48*, 5308–5323.
(17) Dubnikova, I. L.; Berezina, S. M.; Korolev, Y. M.; Dim, G. M.; Lomakin, S. M. *J. Appl. Polym. Sci.* **2007**, *105*, 3834–3850.
(18) Treece, M. A.; Zhang, W.; Moffitt, R. D.; Oberhauser, J. P. *Polym. Eng. Sci.* **2007**, *47*, 898–911.
(19) Kawasumi, M.; Hasegawa, N.; Kato, M.; Usuki, A.; Okada, A. *Macromolecules* **1997**, *30*, 6333–6338.
(20) Nam, P. H.; Maiti, P.; Okamoto, M.; Kotaka, T.; Hasegawa, N.; Usuki, A. *Polymer* **2001**, *42*, 9633–9640.
(21) Lu, Q. W.; Macosko, C. W. *Polymer* **2004**, *45*, 1981–1991.
(22) Varela, C.; Rosales, C.; Perera, R.; Matos, M.; Poirier, T.; Blunda, J.; Rojas, H. *Polym. Compos.* **2006**, *27*, 451–460.
(23) Kissinger, J. B.; Hughes, R. E. *J. Phys. Chem.* **2002**, *63*, 1959.
(24) Liang, Z. M.; Yin, J.; Xu, H. J. *Polymer* **2003**, *44*, 1391–1399.
(25) Rodriguez-Medellin, F. J.; Mata-Padilla, J. M.; Hsiao, B. S.; Waldo-Mendoza, M. A.; Vargas-Ramirez, E.; Baldes-Sanchez, S. *Polym. Eng. Sci.* **2007**, *47*, 1889–1897.
(26) Kilcoyne, A. L. D.; Tyliszczak, T.; Steele, W. F.; Fakra, S.; Hitchcock, P.; Franck, K.; Anderson, E.; Harteneck, B.; Rightor, E. G.; Mitchell, G. E.; Hitchcock, A. P.; Yang, L.; Warwick, T.; Ade, H. *J. Synchrotron Radiat.* **2003**, *10*, 125–136.
(27) Turner-Jones, A.; Aizlewood, J. M.; Beckett, D. R. *Macromol. Chem.* **1964**, *75*, 134–158.
(28) Avrami, M. *J. Chem. Phys.* **1940**, *8*, 212–224.
(29) Golebiewski, J.; Galeski, A. *Compos. Sci. Technol.* **2007**, *67*, 3442–3447.
(30) www.nanoclay.com.
(31) Hotta, S.; Paul, D. R. *Polymer* **2004**, *45*, 7639–7654.
(32) Araki, T.; Ade, H.; Stubbs, J. M.; Sundberg, D. C.; Mitchell, G. E.; Kortright, J. B.; Kilcoyne, A. L. D. *Appl. Phys. Lett.* **2006**, *89*, 124106.
(33) Si, M.; Araki, T.; Ade, H.; Kilcoyne, A. L. D.; Fisher, R.; Sokolov, J. C.; Rafailovich, M. H. *Macromolecules* **2006**, *39*, 4793–4801.
(34) Ade, H.; Hitchcock, A. P. *Polymer* **2008**, *49*, 643.
(35) Dhez, O.; Ade, H.; Urquhart, A. *J. Electron Spectrosc. Relat. Phenom.* **2003**, *128*, 85.

JP9049999